Anderson-McMillan prescription for the density of states of liquid iron*

J. J. Olson

Department of Physics, University of California at San Diego, La Jolla, California 92037
and Metals and Ceramics Division, Oak Ridge National Laboratory, Oak Ridge, Tennessee 37830†

(Received 2 June 1975)

An intensive numerical investigation reveals a gross error in the density of states reported in 1967 by Anderson and McMillan. Whereas they obtained a broad double-peaked resonance that appeared sufficiently reasonable to justify their prescription, correct evaluation of their formula yields a single structureless resonance far too narrow to be representative of a transition-metal d band. This conclusion is verified by algebraically reducing their expression for the density of states to a form that is easily evaluated by hand. Anderson and McMillan also err in claiming that their dispersion relation leads to a vanishing wave number at resonance. The zero wave number is on an extraneous branch and would have led to a nonintegrable singularity in their density of states. Evidently the Anderson-McMillan prescription is inadequate as a description of the effects of s-d hybridization on the density of states of transition metals.

I. INTRODUCTION

Several years ago Anderson and McMillan (AM) presented a simple theory for the density of one-electron states in transition metals.[1] Basing their arguments on the newly understood resonant nature of d bands,[2-4] they proposed an application of multiple-scattering theory similar to the more recent coherent potential approximation.[5] Their final result for the density of states purported to capture the essentials of resonant $s-d$ hybridization without reference to the geometrical arrangement of the ions. It has therefore attracted some attention in the area of disordered systems,[6-9] but to my knowledge there is no record in the literature that their prescription has ever been utilized.[10]

This article details an unsuccessful attempt to reproduce the density of states reported by Anderson and McMillan. Section II describes the Anderson-McMillan prescription and quotes their expression for the density of states. Section III exhibits the conflict and localizes its source by comparing the results of intermediate stages of the calculation with the published results of Anderson and McMillan. Section IV presents a numerically independent check of the density of states based on an algebraic simplification of the Anderson-McMillan formula. The existence of extraneous branches of the Anderson-McMillan dispersion relation is demonstrated numerically in Sec. V, and the behavior of the "zero branch" is derived analytically in Sec. VI. Additional evidence supporting the present calculation is given in Sec. VII; conclusions are in Sec. VIII.

II. METHOD OF ANDERSON AND McMILLAN

Anderson and McMillan argue that in first approximation, the behavior of d electrons on a given atom of the liquid is adequately simulated in an energy-dependent potential of the form

$$v(r,E)=\begin{cases} v_{\mathrm{MT}}(r)\,, & r<r_s \\ C(E)\,, & r>r_s\,, \end{cases} \tag{1}$$

where $v_{\mathrm{MT}}(r)$ is an ordinary muffin-tin atomic potential, r_s is the Wigner-Seitz atomic radius, and the complex number $C(E)$ represents a spatially uniform medium chosen to simulate the effect of multiple scattering from the other atoms. To determine $C(E)$, Anderson and McMillan require that a plane wave propagating in C suffer no forward scattering due to the disturbance $v(r,E)-C(E)$. Thus determined, C defines an effective dispersion relation $k_c(E)$ according to

$$k_c^2(E)\equiv E-C(E)\,. \tag{2}$$

The subscript in Eq. (2) and the following is to remind the reader that k_c is the complex wave number in the medium $C(E)$.

The density of states per atom is determined from the Green's function for the potential $v(r,E)$ by restricting the trace to the interior of the Wigner-Seitz sphere; i.e.,

$$\rho(E)=-\frac{\mathrm{Im}}{\pi}\int_{r\le r_s} G(\vec{\mathrm{r}},\vec{\mathrm{r}},E)\,d^3r\,. \tag{3}$$

Here the Green's function is defined by the differential equation

$$[E+\nabla^2-v(r,E)]\,G(\vec{\mathrm{r}},\vec{\mathrm{r}}',E)=\delta(\vec{\mathrm{r}}-\vec{\mathrm{r}}')\,, \tag{4}$$

with the boundary condition that G consists only of outgoing waves outside the Wigner-Seitz sphere. The spherical symmetry of $v(r,E)$ allows a closed expression for $\rho(E)$ in terms of the atomic logarithmic derivatives at the Wigner-Seitz radius.

Anderson and McMillan give an expression for $\rho(E)$ which will be written here as a sum over angular momenta of a factor $\rho_l(E)$, which is independent of the choice of k_c, times a factor $\mathrm{Im}a_l(E,k_c)$, which contains the effect of k_c,

$$\rho(E)=\sum_l \rho_l(E)\,\mathrm{Im}a_l(E,k_c)\ . \tag{5}$$

As given in Eq. (AM 4.1),

$$\rho_l(E)=\frac{\kappa}{\pi}(2l+1)\int_0^{r_s}\mathcal{J}_l^2(\kappa,r)\,r^2\,dr$$
$$=\frac{1}{\pi}(2l+1)\left(\frac{d\delta_l}{dE}-\tfrac{1}{2}\,r_s^2\,\mathcal{J}_l^2(\kappa,r_s)\frac{\partial\gamma_l(\kappa,\delta_l,r_s)}{\partial\kappa}\right), \tag{6}$$

where $\kappa^2=E$ and $\mathcal{J}_l(\kappa,r)$ is a regular solution of the radial Schroedinger equation for the muffin-tin atom (AM 2.9′),

$$\left(-\frac{1}{r^2}\frac{d}{dr}r^2\frac{d}{dr}+v_{\mathrm{MT}}(r)+\frac{l(l+1)}{r^2}\right)\mathcal{J}_l(\kappa,r)=E\,\mathcal{J}_l(\kappa,r)\ . \tag{7}$$

In addition, δ_l is the phase shift of $\mathcal{J}_l$ in the muffin-tin plateau region ($r_m<r<r_s$), where $\mathcal{J}_l$ is normalized such that (AM 2.11)

$$\mathcal{J}_l(\kappa,r)=\cos\delta_l\,j_l(\kappa r)-\sin\delta_l\,n_l(\kappa r)\ ,\quad r_m<r<r_s\ , \tag{8}$$

and γ_l is the logarithmic derivative of $\mathcal{J}_l$ at the Wigner-Seitz radius (AM 2.2)

$$\gamma_l=\gamma_l(E,r_s)$$
$$=\frac{d}{dr}\ln\mathcal{J}_l(\kappa,r)\Big|_{r=r_s}\ . \tag{9}$$

In the last part of Eq. (6), γ_l is to be formally regarded as a function of κ, δ_l, and r_s (AM 2.1),

$$\gamma_l=\gamma_l(\kappa,\delta_l,r_s)$$
$$=\kappa\frac{\cos\delta_l\,j_l'(\kappa r_s)-\sin\delta_l\,n_l'(\kappa r_s)}{\cos\delta_l\,j_l(\kappa r_s)-\sin\delta_l\,n_l(\kappa r_s)}\ . \tag{10}$$

The derivative of Eq. (10) with respect to κ is to be taken at fixed δ_l and r_s. This completes the specification of $\rho_l(E)$.

The quantity a_l is defined in terms of an irregular solution $\mathfrak{N}_l(\kappa,r)$ of the radial equation, (7). The required normalization is such that on the muffin-tin plateau (AM 2.14),

$$\mathfrak{N}_l(\kappa,r)=\sin\delta_l\,j_l(\kappa r)+\cos\delta_l\,n_l(\kappa r)\ ,$$
$$r_m<r<r_s\ . \tag{11}$$

Now a_l is determined so that the linear combination $\mathfrak{N}_l(\kappa,r)-a_l\mathcal{J}_l(\kappa,r)$ ($r\le r_s$) matches smoothly onto an outgoing wave in the dispersive medium outside r_s. Matching logarithmic derivatives of $\mathfrak{N}_l-a_l\mathcal{J}_l$ and $h_l(k_c r)$, we have (AM 4.5)[11]

$$\left.\frac{(d/dr)\mathfrak{N}_l(\kappa,r)-a_l(d/dr)\mathcal{J}_l(\kappa,r)}{\mathfrak{N}_l(\kappa,r)-a_l\mathcal{J}_l(\kappa,r)}\right|_{r=r_s}=\gamma_l^c\ , \tag{12}$$

where

$$\gamma_l^c\equiv k_c\frac{h_l'(k_c r_s)}{h_l(k_c r_s)}\ , \tag{13}$$

and

$$h_l=j_l+in_l\ . \tag{14}$$

As a check on the sign of a_l, we may take the free boundary condition $k_c=\kappa$ (no medium outside). It is easily checked using the above expressions for $\mathcal{J}_l$ and $\mathfrak{N}_l$ (AM 2.11 and AM 2.14) that

$$\mathfrak{N}_l(\kappa,r)-i\mathcal{J}_l(\kappa,r)-i\,e^{i\delta_l}h_l(\kappa r)\ ,\quad r>r_m\ , \tag{15}$$

so that $a_l=i$ and $\mathrm{Im}a_l=1$ when $k_c=\kappa$.

To complete the AM prescription, one must specify the complex wave number $k_c(E)$. This is determined by requiring that the forward scattering element of the t matrix vanish (AM 3.7),

$$\frac{1}{k_c}\sum_l(2l+1)\,e^{i\delta_l^c}\sin\delta_l^c=0\ , \tag{16}$$

where δ_l^c is the complex phase shift of the regular solution of the radial equation in the dispersive medium outside r_s. In terms of the logarithmic derivative $\gamma_l(E,r_s)$, the complex phase shift is given by (AM 3.6)

$$\cot\delta_l^c(k_c,E)=\frac{k_c\,n_l'(k_c r_s)-\gamma_l(E,r_s)\,n_l(k_c r_s)}{k_c\,j_l'(k_c r_s)-\gamma_l(E,r_s)\,j_l(k_c r_s)}\ . \tag{17}$$

III. COMPARISON OF RESULTS

Every effort has been made to ensure comparability of the present calculation with that of AM. As input for the calculation, Mattheiss has kindly furnished a table of logarithmic derivatives for the iron potential used in his band-structure calculations.[12] This table is believed to be the same as was supplied to Anderson and McMillan. Equations (5) *et seq.* were encoded for computation as in AM wherever such indication was given. Details of the present calculation may be found in Appendix A.

Figure 1 compares the results of the present calculation with the density of states[13] published by Anderson and McMillan. The disagreement is startling. Whereas AM found a split resonance with a full width at half height of 0.28 Ry, I obtain a single peak whose width is only 0.016 Ry. This is an order of magnitude narrower than the d bands in bcc crystalline iron, whose typical spread is 0.32 Ry.[12] Despite its narrow shape, the present $\rho(E)$ envelopes more states (5.7 states on the interval shown in Fig. 1, not counting spin) than does the AM result (4.2 states on the same interval). The remainder of this section will demonstrate that the discrepancy illustrated in Fig. 1 arises during the numerical evaluation of the coefficient $\mathrm{Im}a_2$, which incorporates the effects of the medium $C(E)$.

We first examine $\rho_2(E)$, which is completely independent of the medium. Since $\mathrm{Im}a_l$ is unity when k_c is set equal to κ, we see that $\rho_l(E)$ is the lth contribution to the density of states when the medium is replaced by free space. Thus $\rho_2(E)$ de-

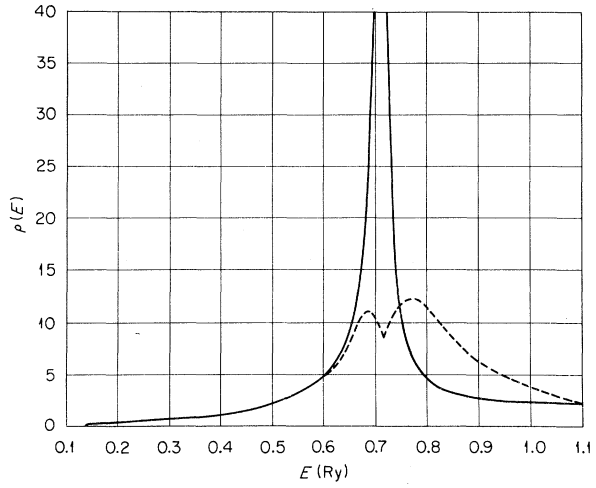

FIG. 1. Density of states of iron according to the Anderson-McMillan prescription, as calculated in the present work (solid line) and by Anderson and McMillan (dashed line read from AM Fig. 5). The present $\rho(E)$ is not singular but reaches a well-defined maximum of $\sim 130.9\ \mathrm{Ry}^{-1}$ at $E = 0.7135$ Ry.

scribes the shape of the bare atomic d resonance. The present calculation of $\rho_2(E)$ is compared in Fig. 2 with the published results of AM. Evidently, $\rho_2(E)$ cannot be the source of disagreement.

Before evaluating a_l, it is necessary to determine the complex wave number $k_c(E)$ as defined by Eqs. (16) and (17). As can be seen from Fig. 3, the present calculation of $k_c(E)$ is substantially the same as in AM. The only difference of note is that AM claims that both $\mathrm{Re}k_c$ and $\mathrm{Im}k_c$ vanish at resonance. This point of disagreement will be considered later in Secs. V and VI. For the present it is sufficient to note that this disagreement is

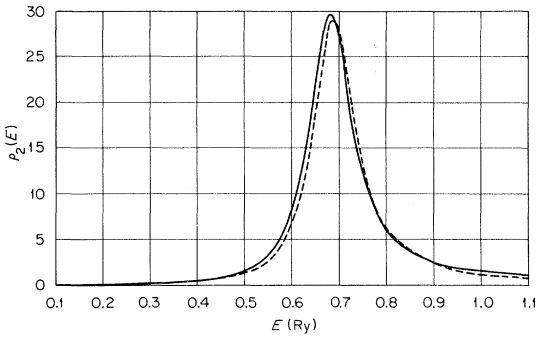

FIG. 2. $l=2$ contribution to the density of states in the absence of the effective medium. The present calculation of Eq. (6) for $\rho_2(E)$ (solid line) is compared with AM Fig. 1 (dashed line).

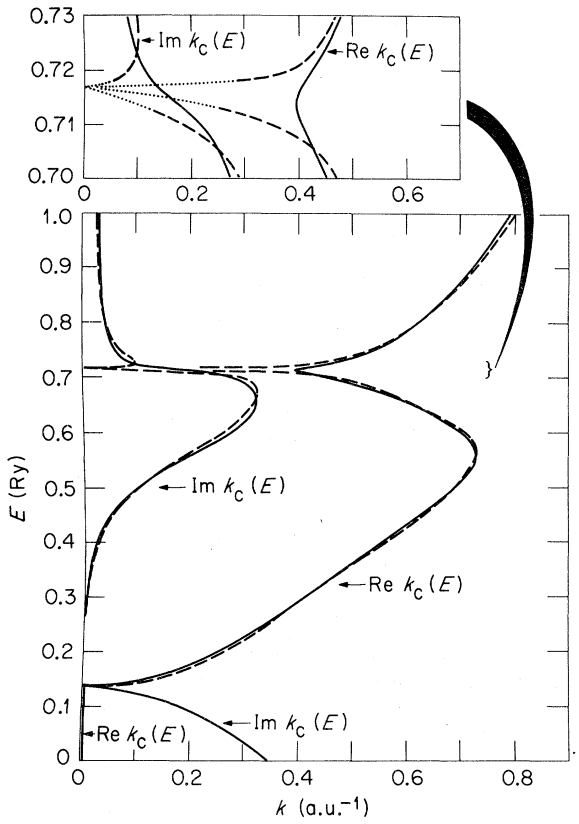

FIG. 3. Complex dispersion relation for the Anderson-McMillan effective medium as calculated in the present work (solid lines) and by Anderson and McMillan (dashed lines read from AM Fig. 2). The disputed behavior of $k_c(E)$ at resonance is shown on an energy scale expanded by a factor of 10. The dotted lines at resonance were inferred from the text of AM and are therefore only schematic.

restricted to a narrow range of energies (0.705 to 0.725 Ry) and thus cannot account for the significant disparity in the densities of states at energies such as 0.8 Ry where there is no discernable disagreement in the dispersion relations.

All that remains is the calculation of $\mathrm{Im}a_l$ from

$$a_l = \frac{(d/dr)\mathfrak{N}_l - \gamma_l^c \mathfrak{N}_l}{(d/dr)\mathfrak{J}_l - \gamma_l^c \mathfrak{J}_l} \tag{18}$$

$$= \frac{\cot\delta_l[\kappa n_l'(\kappa r_s) - \gamma_l^c n_l(\kappa r_s)] + [\kappa j_l'(\kappa r_s) - \gamma_l^c j_l(\kappa r_s)]}{\cot\delta_l[\kappa j_l'(\kappa r_s) - \gamma_l^c j_l(\kappa r_s)] - [\kappa n_l'(\kappa r_s) - \gamma_l^c n_l(\kappa r_s)]} . \tag{19}$$

The results for $l=2$ are graphed in Fig. 4, and tabulated values at three key energies are given in Table I. Evidently the origin of the disagreement is buried somewhere in the evaluation of Eq. (19). The computer codes that generated the present calculation of $\mathrm{Im}a_2$ were verified by machine

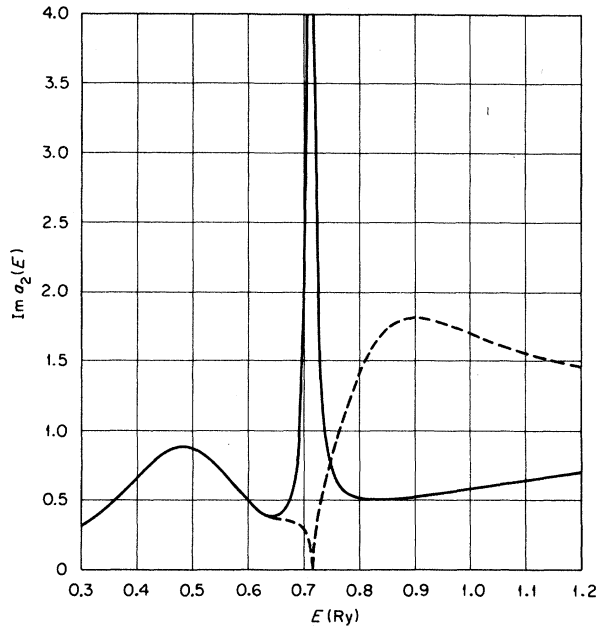

FIG. 4. Factor Im a_2 which modifies the $l=2$ contribution to $\rho(E)$ to account for the effective medium, as calculated in the present work (solid line) and by Anderson and McMillan (dashed line read from AM Fig. 6).

evaluation in the limit $k_c=\kappa$ (where $a_l=i$) and by hand evaluation using the computed $k_c(E)$.

IV. NUMERICALLY INDEPENDENT CHECK

This section will develop and evaluate an expression for $\rho(E)$ which is mathematically equivalent to the Anderson-McMillan expression but which is so different with regard to numerical implementation as to constitute an independent check on the calculation.

Equations (5) and (6) for the Anderson-McMillan density of states can be combined as in (AM 4.1) to read[14]

$$\rho(E)=\frac{1}{\pi}\sum_l (2l+1)\int_0^{r_s} \mathcal{J}_l^2(\kappa, r)r^2\,dr\,\mathrm{Im}\kappa a_l\,. \quad (20)$$

A greatly simplified formula for $\rho(E)$ results if one employs the following two identities:

$$\int_0^{r_s} \mathcal{J}_l^2(\kappa, r)r^2\,dr=-[r_s^2\mathcal{J}_l^2(\kappa, r_s)]\frac{d\gamma_l}{dE}\,, \quad (21)$$

$$\mathrm{Im}\kappa a_l=[r_s^2\mathcal{J}_l^2(\kappa, r_s)]^{-1}\,\mathrm{Im}\frac{1}{\gamma_l-\gamma_l^c}\,. \quad (22)$$

The first of these was proved by Anderson and McMillan (cf. AM 2.20). Proof of the second is as follows:

Start with Eq. (18) for a_l and factor out $\mathfrak{N}_l$ and $\mathcal{J}_l$ to leave

$$a_l=\frac{\mathfrak{N}_l}{\mathcal{J}_l}\frac{\tilde{\gamma}_l-\gamma_l^c}{\gamma_l-\gamma_l^c}\,, \quad (23)$$

where $\tilde{\gamma}_l$ stands for the logarithmic derivative of $\mathfrak{N}_l$ at $r=r_s$,

$$\tilde{\gamma}_l=\frac{(d/dr)\mathfrak{N}_l}{\mathfrak{N}_l}\,, \quad (24)$$

and where γ_l is familiar as the logarithmic derivative of $\mathcal{J}_l$. The trick is to express $\tilde{\gamma}_l$ in terms of both γ_l and the Wronskian of $\mathcal{J}_l$ and $\mathfrak{N}_l$,

$$\begin{aligned}\tilde{\gamma}_l&=\gamma_l+\frac{(d/dr)\mathfrak{N}_l}{\mathfrak{N}_l}-\frac{(d/dr)\mathcal{J}_l}{\mathcal{J}_l}\\&=\gamma_l+\left(\mathcal{J}_l\frac{d}{dr}\mathfrak{N}_l-\mathfrak{N}_l\frac{d}{dr}\mathcal{J}_l\right)\Big/(\mathcal{J}_l\mathfrak{N}_l)\\&=\gamma_l+(\kappa r_s^2\mathcal{J}_l\mathfrak{N}_l)^{-1}\,. \end{aligned}\quad (25)$$

The last equality follows from the known forms of $\mathcal{J}_l$ and $\mathfrak{N}_l$ on the interval $r_m\le r\le r_s$ [Eqs. (8) and (11)]. Substituting this expression for $\tilde{\gamma}_l$ into Eq. (23) gives

$$\kappa a_l=\kappa\frac{\mathfrak{N}_l}{\mathcal{J}_l}+(r_s^2\mathcal{J}_l^2)^{-1}\frac{1}{\gamma_l-\gamma_l^c}\,. \quad (26)$$

The proof is completed by noting that $\kappa\mathfrak{N}_l/\mathcal{J}_l$ and $\mathcal{J}_l^2$ are real. This is obvious for positive energies and is easily verified for negative energies by using the analytic continuation of Eqs. (8) and (11) to imaginary κ.

Inserting the identities (21) and (22) into Eq. (20) effects a cancellation of the terms involving $\mathcal{J}_l^2(\kappa, r_s)$, so that the Anderson-McMillan formula for the density of states is reduced to

$$\rho(E)=-\frac{\mathrm{Im}}{\pi}\sum_l (2l+1)\frac{d\gamma_l/dE}{\gamma_l-\gamma_l^c}\,. \quad (27)$$

TABLE I. Sample results of the present calculation at three key energies. $E=0.68$ and $E=0.80$ correspond roughly to the two peaks in $\rho(E)$ found by AM, and $E=0.714$ to the single peak in the present $\rho(E)$.

E(Ry)	k_c(a.u.$^{-1}$)	a_2	ρ_2 Im a_2	ρ [Eq. (5)]	ρ (AM Fig. 5)
0.680	(0.531, 0.312)	(0.982, 0.637)	18.96	19.88	11.0
0.714	(0.396, 0.174)	(−0.540, 5.886)	128.9	130.1	8.0
0.800	(0.622, 0.042)	(−0.568, 0.513)	3.203	4.538	11.5

TABLE II. Sample calculations of the $l=2$ density of states from the simplified Anderson-McMillan formula, Eq. (27). γ_2^c was calculated from Eq. (28) using the values of k_c given in Table I.

E(Ry)	γ_2	$d\gamma_2/dE$	γ_2^c	Im $(\gamma_2-\gamma_2^0)^{-1}$	Eq. (27) $l=2$
0.680	−0.7375	−8.165	(−1.077, 0.2955)	1.459	18.96
0.714	−1.085	−12.71	(−1.045, 0.1461)	6.371	128.9
0.800	−4.110	−99.43	(−0.810, 0.2214)	0.02024	3.203

The simplicity of this formula is particularly significant in the present context as it greatly reduces the possibility of computational error.

In fact, given $k_c(E)$, it is now trivial to calculate $\rho(E)$. The real logarithmic derivatives of the muffin-tin wave functions can be read from a table, and the complex logarithmic derivatives of the Hankel functions can be computed without the use of transcendental functions,[15] e.g., for $l=2$,

$$\gamma_2^c = ik_c - \frac{1}{r_s}\,\frac{(k_c r_s)^2 + 6ik_c r_s - 9}{(k_c r_s)^2 + 3ik_c r_s - 3}\,. \tag{28}$$

The results of using Eq. (28) to calculate the $l=2$ contribution to Eq. (27) are listed in Table II. Note that the results of this calculation agree to four significant figures with the values of $\rho_2 \operatorname{Im} a_2$ listed in Table I even at the peak of the resonance. This agreement verifies that the present $\rho(E)$ has been correctly calculated from $k_c(E)$.

V. EXTRANEOUS BRANCHES OF $k_c(E)$

There remains only the question of the precise behavior of $k_c(E)$ at resonance. Although the discrepancy in $k_c(E)$ shown in Fig. 3 appears slight, it nevertheless invites suspicion of multiple branches in the dispersion relation and of the possibility of switching to a branch that passes through zero k_c at resonance. In this section, the complex k_c plane will be fully illuminated to show that although such a "zero branch" does exist, it is quite distinct from the branch illustrated by the solid line in Fig. 3.

We begin with a study of the analytic properties of the Anderson-McMillan t matrix $t(z, E)$ as a function of the complex variable $z = k_c r_s$ at a fixed energy E. $t(z, E)$ is defined as the sum over l of

$$t_l(z, E) = \frac{2l+1}{k_c r_s}\, e^{i\delta_l^c} \sin\delta_l^c$$

$$= \frac{2l+1}{z}\, i\,\frac{z j_l'(z) - \gamma_l(E, r_s) r_s j_l(z)}{z h_l'(z) - \gamma_l(E, r_s) r_s h_l(z)}\,. \tag{29}$$

Equation (29) follows from Eqs. (A5) and (17). The small-z behavior is best displayed by rearranging the spherical functions as

$$j_l(z) = z^l \tilde{j}_l(z)\,, \tag{30}$$

$$h_l(z) = \frac{e^{iz}}{iz^{l+1}}\,\tilde{h}_l(z)\,. \tag{31}$$

Here $\tilde{j}_l$ is an infinite series in z^2, and $\tilde{h}_l$ is a polynominal of degree l in iz,

$$\tilde{j}_l(z) = \frac{1}{(2l+1)!!}\left(1 - \frac{z^2}{2(2l+3)} + \cdots\right),$$

$$\tilde{h}_0(z) = 1, \quad \tilde{h}_1(z) = 1 - iz\,, \tag{32}$$

$$\tilde{h}_2(z) = 3 - 3(iz) + (iz)^2\,.$$

Equations (30) and (31) together with the recursion relations for the derivatives of j_l and h_l allow the following form for $t_l(z, E)$:

$$e^{iz} t_l(z, E) = (2l+1) z^{2l}\,\frac{(l - \gamma_l r_s)\tilde{j}_l - z^2 \tilde{j}_{l+1}}{(l+1+\gamma_l r_s)\tilde{h}_l - z^2 \tilde{h}_{l-1}}\,. \tag{33}$$

For $l=0$, $\tilde{h}_{l-1}$ is to be interpreted as $-1/iz$.

Let $q_l(z, E)$ and $p_l(z, E)$, respectively, represent the numerator and denominator of the quotient in Eq. (33). So q_l is an infinite series in z^2 and p_l is a polynominal of degree $(l+1)$ in iz. Both q_l and p_l are analytic in z [except, of course, when $\gamma_l(E, r_s) = \infty$]. With these definitions, $t(z, E)$ is written as

$$e^{iz} t(z, E) = \frac{q_0}{p_0} + 3z^2\,\frac{q_1}{p_1} + 5z^4\,\frac{q_2}{p_2}\,, \tag{34}$$

where contributions from $l \geq 3$ have been discarded in keeping with Anderson-McMillan. Now $t(z, E)$ will have poles arising from the $l+1$ roots of each $p_l(z, E)$. As these poles tend to complicate the numerical task of locating the zeroes of $t(z, E)$, it is preferable to study the analytic function $f(z, E)$ defined by

$$f(z, E) = e^{iz} t(z, E)\, p_0 p_1 p_2$$

$$= q_0 p_1 p_2 + 3z^2 q_1 p_0 p_2 + 5z^4 q_2 p_0 p_1\,. \tag{35}$$

Evidently, $f(z, E)$ has the same zeroes as $t(z, E)$ but without the poles.

The structure of $f(z, E)$ is illustrated in Fig. 5. The solid and dashed lines, respectively, are preimages in the z plane of the real and imaginary axes of the complex f plane. In other words, $f(z, E)$ is purely real for z on a solid line, purely imaginary on a dashed line, and thus zero at an intersection. The lines were located numerically by evaluating Eq. (35) on a fine grid of points in the z plane. The analyticity of f requires that each zero in a bounded region give rise to four lines exiting that region. This fact, together with the

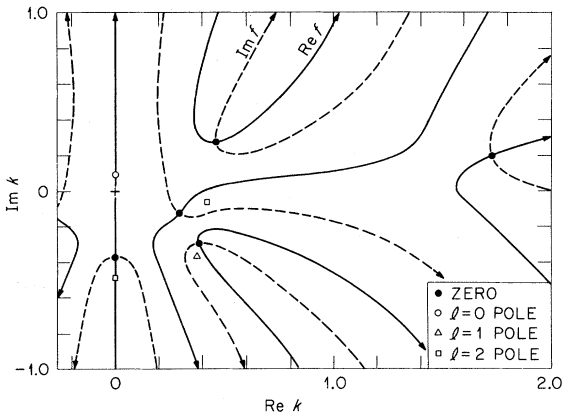

FIG. 5. Structure of the analytic part $f(z,E)$ of the Anderson-McMillan t matrix $t(z,E)$ as a function of the complex variable $k=z/r_s$ at a fixed energy $E=0.70$ Ry. $f(z,E)$ is real on the solid lines, imaginary on the dashed lines, and hence, zero at their intersections. The arrows indicate the directions of increasing Ref or Imf. The locations of the poles to $t_l(z,E)$ are shown for $l=0$, 1, 2.

fineness of the grid ($\Delta k=0.02$ a.u.$^{-1}$), as compared to the apparent scale of variation of f ($\delta k \sim 0.1$ a.u.$^{-1}$), indicates *there are no other zeroes of f in the region illustrated.*

Of the five zeroes revealed by Fig. 5, only one is acceptable in a dispersion relation. Three lie in the lower half plane in the vicinity of the poles of $t_2(z,E)$ and $t_1(z,E)$. These three may be rejected as describing exponentially growing waves; we expect waves that are damped by disorder. The two zeroes in the upper half plane are but the beginning of an infinite sequence of zeroes stretching out along the real axis and spaced asymptotically by $\Delta k_c=\pi/r_s$.[16] All but the first of these can be rejected as not reducing to the correct free-electron limit. Mathematically, the infinity of zeroes arises from the approximate periodicity of $j_l(k_c r_s)$ and $h_l(k_c r_s)$ at large real arguments. Physically, it is an artifact of allowing unbounded alterations of the potential outside the Wigner-Seitz sphere even in the nearly-free-electron limit. The one zero in Fig. 5 not thus dismissed is at Re$k_c \sim 0.45$ and Im$k_c \sim 0.27$, in agreement with the values found in AM at $E=0.70$ Ry (cf. Fig. 3).

As the energy is varied, the zeroes of $t(z,E)$ trace out trajectories in the complex z plane, as shown in Fig. 6. The motion was followed numerically by an automatic routine in energy steps as small as 0.0001 Ry and was checked by making plots of the type in Fig. 5 at over two dozen selected energies. The simple loop in the upper right-hand quadrant represents the same data as the solid lines in Fig. 3. The AM data also follow this loop, except for the portion drawn as an arrow. Anderson and McMillan would replace this smooth segment with a path bending sharply to the origin and back.

Although the present calculation confirms that $z=0$ is a solution to $t(z,E)=0$, Fig. 6 shows that this solution belongs to trajectories originating in the lower half plane. Moreover, there is no indication that the AM result for $k_c(E)$ actually follows one of these trajectories through the origin; if it did, k_c would have been pure imaginary upon leaving the origin and there would have been a finite gap in the density of states (cf. Sec. VI).

VI. ANALYSIS AT SMALL k_c

This section will demonstrate that a careful expansion of the AM dispersion relation in the limit of vanishing k_c yields precisely the form of the two symmetrical zero branches shown in Fig. 6. Moreover, this same expansion when applied at small but finite k_c also yields the nonzero branch shown in Fig. 3, thus verifying the existence of both branches at the same energy. The form of the density of states for the zero branch is also derived.

Under what conditions is a zero branch possible? Inspection of Eq. (34) for $e^{i\delta_l}t(z,E)$ shows that $t(0,E)$ vanishes only if (i) $q_0(0,E)=0$, or if (ii) $p_l(z,E)$ vanishes like z^{2l} for some $l>0$. The first case is identical to the Wigner-Seitz condition

$$\gamma_0(E^{\mathrm{WS}}, r_s)=0\,, \tag{36}$$

and determines the energy $E^{\mathrm{WS}}=0.136$ Ry at the bottom of the band in Fig. 3. The second case requires that for some $l>0$,

$$l+1+\gamma_l(E^{\mathrm{AM}}, r_s)r_s=0\,. \tag{37}$$

On the energy range from zero to 1.25 Ry, this condition is met only for $l=2$ and determines the

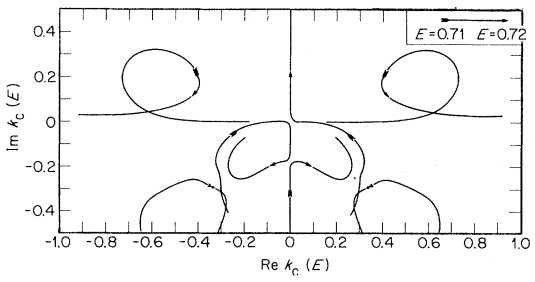

FIG. 6. Trajectories in the complex plane of the zeroes of $t(z,E)$ from $E=0.15$ to 0.125 Ry ($z=k_c r_s$). The arrows indicate the motion of the zeroes as the energy is increased through resonance from 0.71 to 0.72 Ry. The right-angle bends formed when two trajectories meet simultaneously on the imaginary axis have been rounded to show one of the allowable choices of connectivity.

energy $E^{AM} = 0.7171$ Ry, which may be inferred to be the energy at which Anderson and McMillan claim $k_c(E)$ goes to zero [note that this energy differs slightly from the energy $E_{res} = 0.7135$ at which the present $\rho(E)$ reaches maximum]. It will be convenient to introduce the notation

$$\epsilon = -3 - \gamma_2(E, r_s) r_s , \tag{38}$$

so that

$$p_2(z, E) = -\epsilon \tilde{h}_2(z) - z^2 \tilde{h}_1(z) . \tag{39}$$

In the vicinity of E^{AM}, ϵ is proportional to the energy difference $E - E^{AM}$ with a constant proportionality of 35.3 Ry^{-1}. Thus ϵ may be thought of as a dimensionless energy parameter.

The dispersion relation is obtained by setting $t(z, E) = 0$ in Eq. (34). In the limit of small ϵ and small z, the contributions from both $l = 0$ and $l = 2$ will be of order unity, the remaining terms contributing $O(z^2)$, so that z as a function of ϵ is determined by

$$\frac{q_0}{p_0} + 5z^4 \frac{q_2}{p_2} + O(z^2) = 0 . \tag{40}$$

Recalling that p_2 is of $O(z^4)$, we may rearrange Eq. (40) so that the dispersion relation reads

$$p_2 = -5z^4 q_2 p_0 q_0^{-1} [1 + O(z^2)] . \tag{41}$$

Note that through $O(z^3)$, the dispersion relation is equivalent to setting $p_2(z, E) = 0$. To this order, one cannot resolve the separation between the zero and the pole of $t(z, E)$ [hence, the necessity of using $f(z, E)$ for numerical work]. From Eqs. (39) and (32) the dispersion relation to lowest order in z is seen to be

$$\epsilon \sim -z^2/3 , \tag{42}$$

or

$$E \sim E^{AM} - k_c^2/14.9 . \tag{43}$$

Thus just below E^{AM}, the dispersion relation is approximately real and describes an electron with a negative effective mass about 15 times larger than the free mass. For energies just above E^{AM}, however, the wave number is purely imaginary.

The density of states for this branch of the dispersion relation can be obtained from Eq. (27) with greater dispatch if γ_l^c is rewritten in terms of $z h_l'(z)$ and $h_l(z)$, which in turn can be simplified by using Eq. (31). Then Eq. (27) takes on the exact form

$$\rho(E) = -\frac{\mathrm{Im}}{\pi} \sum_l (2l+1) \frac{\tilde{h}_l(z)}{p_l(z, E)} \frac{d\gamma_l r_s}{dE} , \tag{44}$$

where p_l is the same polynomial that appears in the denominator of $t_l(z, E)$ in Eq. (33). Unlike $t_l(z, E)$, however, there is no z^{2l} in the numerator of Eq. (44), so it may be anticipated that $\rho(E)$ will become singular as p_2 vanishes. The precise form of this singularity is determined by taking p_2 as given by the dispersion relation Eq. (41). Then to $O(z^2)$, $\tilde{h}_2$ may be replaced by $3(1 - iz)$, q_0 by $-\gamma_0 r_s$, and q_2 by $\frac{1}{3}$; p_0 is exactly $1 + \gamma_0 r_s - iz$. With these replacements,

$$\frac{\tilde{h}_2}{p_2} = \frac{9}{5} \frac{\gamma_0 r_s}{z^4} \frac{1 - iz}{1 + \gamma_0 r_s - iz} [1 + O(z^2)] . \tag{45}$$

As z^2 is real for small z, the lowest-order term in the above expression will be real and hence not contribute to $\rho(E)$. The density of states arises from the iz terms and is given by

$$\rho(E) \sim \frac{1}{\pi} \left(\frac{-d\gamma_2 r_s}{dE}\right) \left(\frac{3\gamma_0 r_s}{1 + \gamma_0 r_s}\right)^2 \left(\frac{-\mathrm{Re}z}{z^4}\right) . \tag{46}$$

For energies just above E^{AM}, the dispersion relation is purely imaginary and the density of states is identically zero. For energies just below E_{AM}, the density of states becomes singular like

$$\rho(E) \propto \pm (E^{AM} - E)^{-3/2} , \tag{47}$$

where the plus/minus sign applies to the branch of the dispersion relation that approaches the origin in Fig. 6 from the lower left-hand/right-hand quadrant. Note that this singularity is nonintegrable; i.e., the integrated density of states is divergent.

Direct computation of $\rho(E)$ from Eqs. (5) and (6) verifies this behavior. As shown in Fig. 7, $\rho(E)$ consists of two peaks separated by a narrow

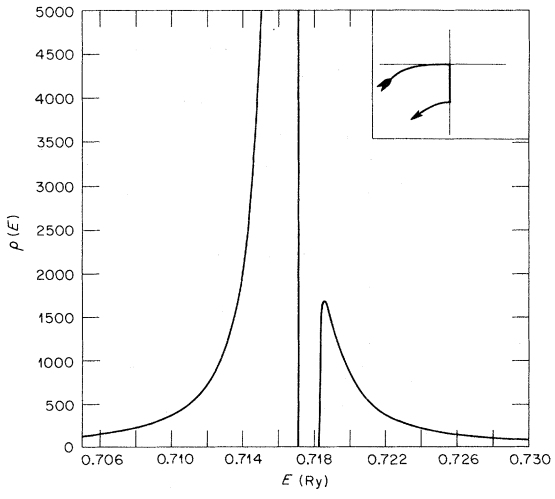

FIG. 7. Density of states that results when the Anderson-McMillan formula is applied to one of the branches of the disperison relation that go to $k_c = 0$ at resonance. The inset identifies the corresponding trajectory in the complex k_c plane. As $k_c \to 0$, $\rho(E)$ becomes singular. Had the mirror image of this trajectory been chosen (cf. Fig. 6), the density of states would have been negative.

gap. The higher energy peak corresponds to the dispersion relation turning away from the negative imaginary axis. It is nonsingular because $p_2(z, E)$ is of order z^4, which is not zero in this case.

Although the preceding small-z analysis yields exact results only when applied to the limiting forms of the zero branch and its density of states, it is also capable of reproducing $k_c(E)$ on the "nonzero" branch. This is most easily demonstrated for $E = E^{\mathrm{AM}}$. Taking $\epsilon = 0$ in Eq. (39) and using the same expressions for q_0, q_2, and p_2 as were used in Eq. (45), the dispersion relation Eq. (40) now reads

$$e^{iz}t(z, E^{\mathrm{AM}}) = \frac{-\gamma_0 r_s}{1+\gamma_0 r_s - \zeta} + \frac{5}{3}\,\frac{\zeta^2}{1-\zeta} = 0\,, \qquad (48)$$

where $\zeta = iz = ik_c r_s$. Equation (48) is equivalent to a cubic polynomial in ζ and can therefore be solved in closed form. Taking $\gamma_0(E^{\mathrm{AM}}, r_s) r_s = -1.40$, the solution of Eq. (48) is $k_c = 0.41 + 0.19i$, in very good agreement with the previously computed value $k_c = 0.4061 + 0.1850i$ shown in Fig. 3.

VII. ADDITIONAL EVIDENCE

Chang and Sher[17] at the college of William and Mary have also attempted to reproduce the Anderson-McMillan density of states starting from Matthiess's logarithmic derivatives. Their calculation of $\mathrm{Im}a_2$, however, verifies my result over the full energy range from zero to 1.20 Ry, except for the interval 0.70 to 0.72 Ry where they conclude that k_c and $\mathrm{Im}a_2$ fall rapidly to zero.

In addition to the results reported here, I have also applied the AM prescription to copper and zinc, in both cases observing the same unphysical effects in the density of states. Moreover, my calculations for copper have been verified by the independent calculations of Butler[18] of the Metals and Ceramics Division, Oak Ridge National Laboratory.

VIII. CONCLUSION

On the basis of the evidence presented above, one may conclude that the rather reasonable-looking density of states reported by AM is not a consequence of their theory but is instead due to a numerical error in the last stages of their calculation. In fact their prescription for the effective medium produces the wrong effect: it narrows the resonance rather than broadening it. The bare resonance $\rho_2(E)$ shown in Fig. 2 has a full width at half maximum of 0.110 Ry, but the AM criterion for the effective medium, Eq. (16), reduces this width by an order of magnitude to 0.016 Ry. Evidently, the Anderson-McMillan prescription is completely inadequate as a description of the effects of $s-d$ hybridization on the density of states of transition metals.

ACKNOWLEDGMENTS

I am grateful to Professor W. Kohn, who introduced me to the work of Anderson and McMillan, and under whose direction the present discrepancy was discovered. Dr. Anderson's patient criticism of an earlier draft of this paper, especially as regards the zero branch, has been most helpful and is greatly appreciated.

APPENDIX: DETAILS OF THE CALCULATION

Tabulated values of $\gamma_l(E, r_m) r_m^2$ for five l values and 25 energies from $E = 0.00$ to 1.20 Ry were obtained from Mattheiss. The muffin-tin radius $r_m = 2.345543$ a.u. and the Wigner-Seitz radius $r_s = 2.667083$ a.u. correspond to a bcc iron lattice with lattice constant $a = 5.6148$ a.u. Each $\gamma_l(E, r_m)$ was converted to $\cot\delta_l(E)$ which, in turn, was converted to $\gamma_l(E, r_s)$ as directed by (AM 5.2) and (AM 5.3). To obtain the necessary energy resolution of 0.0001 Ry in the d band, $\gamma_l(E, r_s)$ was interpolated using an algorithm based on quadratic Lagrangian interpolation of neighboring triplets. For $E > 0.500$ the inverse of $[\gamma_2(E, r_s) - 0.5]$ was interpolated (γ_2 becomes singular at $E = 0.847$).

Energy derivatives of δ_l were coded in terms of numerical derivatives of either $\tan\delta_l$ or $\cot\delta_l$ (whichever was locally most linear in E) according to

$$\frac{d\delta_l}{dE} = (1+\tan^2\delta_l)^{-1}\,\frac{d}{dE}\tan\delta_l \qquad (A1)$$

or

$$\frac{d\delta_l}{dE} = -(1+\cot^2\delta_l)^{-1}\,\frac{d}{dE}\cot\delta_l\,. \qquad (A2)$$

To avoid the singularity of γ_2, the partial derivative of $\gamma_l(\kappa, \delta_l, r_s)$ was reduced algebraically to an expression involving only Wronskians of Bessel functions,

$$-\tfrac{1}{2} r_s^2 \vartheta_l^2\,\frac{\partial\gamma_l}{\partial\kappa} = \tfrac{1}{2} r_s^2\{\cos^2\delta_l[xj_l', j_l] + \sin^2\delta_l[xn_l', n_l] - \cos\delta_l\sin\delta_l([xj_l', n_l] + [xn_l', j_l])\}\,, \qquad (A3)$$

where, for example,

$$[xj_l', n_l] \equiv xj_l'(x)n_l'(x) - [xj_l'(x)]' n_l(x)\big|_{x=\kappa r_s}\,. \qquad (A4)$$

To determine k_c, the forward scattering t matrix Eq. (16) was coded by use of the identity

$$e^{i\delta_l^c}\sin\delta_l^c = (\cot\delta_l^c - i)^{-1}\,, \qquad (A5)$$

where $\cot\delta_l^c$ is given by Eq. (17). As in AM, only $l = 0$, 1, 2 were kept in Eq. (16). Roots of the t matrix were located in three ways: (i) by minimiz-

ing the absolute value squared of the t matrix, (ii) by Müllers method, [19] and (iii) by direct examination of the real and imaginary parts of the t matrix on an array of points in the complex k_c plane.

The coefficient a_l was coded from Eq. (19) with γ_l^c coded as in Eq. (13). It was verified by direct evaluation that these codes correctly yield $\mathrm{Re}a_l = 0$ and $\mathrm{Im}a_l = 1$ when $\mathrm{Re}k_c = \kappa$ and $\mathrm{Im}k_c = 0$.

All the above formulas that require Bessel functions were rewritten for coding in terms of "scaled Bessel functions," e.g.,

$$\tilde{j}_l \equiv s^{-l} j_l(z), \quad \text{etc.}, \tag{A6}$$

where $s = z$ if $|z| < 1$, otherwise $s = 1$. This eliminates roundoff and truncation errors at small arguments by always working with functions that are finite at the origin.

Bessel functions of real argument were calculated from series at small arguments, upward recursion at large arguments, and downward recursion at intermediate arguments according to the algorithm of Corbato and Uretsky.[20] For complex arguments only series were used.

Note added in proof. Although attempts were made in the early stages of this work to locate the Anderson-McMillan computer program, it could not be found until after this work had been submitted for publication. Recently Dr. Anderson and I independently discovered that the AM program indeed has an error, which has the effect of replacing $\cot\delta_l$ in Eq. (19) by the inverse of δ_l. This replacement explains the discrepancy between the densities of states shown in Fig. (1). I thank Dr. Anderson for his active participation in the resolution of this discrepancy. I also acknowledge the support of the National Science Foundation and the Office of Naval Research.

---

*Research sponsored by the U. S. Energy Research and Development Administration under contract with the Union Carbide Corporation, and supported in part by the National Science Foundation and the Office of Naval Research.

†Present address.

[1]P. W. Anderson and W. L. McMillan, *Proceedings of the International School of Physics "Enrico Fermi,"* Course 37, edited by W. Marshall, (Academic, New York, 1967); to be referred to as AM.

[2]J. M. Ziman, Proc. Phys. Soc. 86, 337 (1965).

[3]L. Hodges and H. Ehrenreich, Phys. Lett. 16, 203 (1965).

[4]F. H. Mueller, Phys. Rev. 153, 659 (1967).

[5]P. Soven, Phys. Rev. 156, 809 (1967).

[6]B. L. Gyorffy, Phys. Rev. B 1, 3290 (1970).

[7]L. Schwartz and H. Ehrenreich, Ann. Phys. 64, 100 (1971).

[8]D. House and P. V. Smith, J. Phys. F 3, 753 (1974).

[9]L. M. Roth, Phys. Rev. B 7, 432 (1973).

[10]The work of Schwartz and Ehrenreich (Ref. 7) is similar but differs in the choice of the effective medium.

[11]Equation (AM 4.5) contains a trivial error in the sign of a_l which has been corrected here to be consistent with the previously quoted formulas. The same error appears in (AM 2.15) where it is incorrectly stated that $\mathcal{F}_l + i\mathcal{G}_l \to e^{i\delta_l} h_l$.

[12]L. F. Mattheiss, Phys. Rev. 134, A970 (1964).

[13]The density of states curves in AM Fig. 1 and AM Fig. 5 count spin, whereas the corresponding formulas in AM do not. The AM data have therefore been divided by two for comparison with the present results.

[14]AM 4.1 uses the form $\kappa\mathrm{Im}\,a_l$ which applies only to positive energies. The correct form for both negative and positive E is $\mathrm{Im}\,\kappa a_l$ as in Eq. (20).

[15]The factored form of h_l in Eq. (31) shows why γ_l^c in Eq. (28) is so simple: $\ln h_l$ contains no exponentials.

[16]This asymtotic value for the spacing is an artifact of truncating $t(z, E)$ at finite l.

[17]K. S. Chang and A. Sher (private communication).

[18]W. H. Butler (private communication).

[19]D. E. Müller, Mathematical Tables and Aids to Computation 10, 208 (1956).

[20]F. J. Corbató and J. L. Uretsky, J. Assoc. Comput. Mach. 6, 366 (1959).